Creating nanoscale Ag patterns on the Si(111)–($\sqrt{3} \times \sqrt{3}$)*R*30°-Ag surface via guided self-assembly

Alex Belianinov
The Ames Laboratory and Department of Chemistry, Iowa State University, Ames, Iowa 50011

Barış Ünal[a)]
The Ames Laboratory and Department of Material Science and Engineering, Iowa State University, Ames, Iowa 50011

Michael C. Tringides
The Ames Laboratory and Department of Physics and Astronomy, Iowa State University, Ames, Iowa 50011

Patricia A. Thiel[b)]
The Ames Laboratory, Department of Chemistry, and Department of Material Science and Engineering, Iowa State University, Ames, Iowa 50011

(Received 27 February 2012; accepted 29 June 2012; published 20 July 2012)

Patterns of Ag nanostructures can be created on the Si(111)–($\sqrt{3} \times \sqrt{3}$)*R*30°-Ag surface, using a simple two-step process in ultrahigh vacuum. First, patterns are created using the tip of a scanning tunneling microscope. Second, Ag is deposited at room temperature. The Ag diffuses over long distances on the surface and selectively aggregates at the patterned regions. The size of the Ag features is ~3–4 nm. © *2012 American Vacuum Society*. [http://dx.doi.org/10.1116/1.4738745]

I. INTRODUCTION

Patterning surfaces at the nanometer scale is an extremely active, broad field of research, with potential and real impact in many areas.[1–4] An important subset of the area of nanopatterning consists of creating shapes, such as dots and lines, of metals on semiconductor surfaces, using a scanning tunneling microscope (STM).[3,5–7] In this letter we describe a new way of patterning a specific Ag-rich surface phase of Si(111) using an STM tip. The constituents of the patterns are nanometer-scale clusters of Ag.

The system Ag/Si is attracting interest because of the optical properties of silver nanoparticles or films, in or on Si. Possible applications include photovoltaics,[8] fiber optics,[9] and photonic band gap devices.[10] In addition to its optical properties, silver is advantageous in such technologies because of its immiscibility with silicon, a feature that is unusual among transition metals. This allows Ag and Si to be combined, while retaining aspects of their individual properties.

The Ag-rich surface phase that we start with is denoted ($\sqrt{3} \times \sqrt{3}$)*R*30°—$\sqrt{3}$ for short—and it has been investigated extensively.[11–19] The following facts are most germane to the present investigation. The $\sqrt{3}$ forms from the Si(111)-(7 × 7) at temperatures in the range 500–800 K, and contains 1.0 monolayer (ML) of Ag. Exactly 1.06 ML of Si is displaced when the $\sqrt{3}$ forms. This displacement leads to $\sqrt{3}$ holes and $\sqrt{3}$ islands that are above and below the level of the original (7 × 7), respectively.[11,12,14–19] The island–hole structure will be evident in most of the STM images shown in this letter.

In previous work, we investigated diffusion and nucleation of Ag deposited on the $\sqrt{3}$ in a temperature range of 50–300 K. At 300 K, we found that Ag can diffuse freely over the island–hole boundaries.[20] In fact, it can diffuse over distances of at least 1 μm, if the surface is completely covered by $\sqrt{3}$. If it is not completely covered by $\sqrt{3}$, regions of the Si(111)-(7 × 7) selectively trap Ag. The long diffusion length on the $\sqrt{3}$ was attributed to a moderate diffusion barrier of 0.2 eV, plus a critical size greater than 1 for homogeneous nucleation at this temperature.[20,21]

The idea of patterning the $\sqrt{3}$ surface was triggered by our discovery that the diffusing Ag becomes selectively trapped at step-bunch regions, even though these regions are widely separated from one another.[20] At the step-bunch regions, the excess Ag forms three-dimensional islands. As the step-bunch regions can be thought of as defect-dense areas, we decided to investigate whether *artificial* defects (tip-induced disruptions in the $\sqrt{3}$) might also act as selective traps for Ag.

The creation of defects on the $\sqrt{3}$ surface, using an STM tip, has been demonstrated previously by Riehl-Chudoba *et al.*[22] (henceforth, RCRG). They applied voltage pulses that were positive with respect to the sample. By controlling the magnitude of the voltage pulse, they could remove only the top layer of Ag atoms in the $\sqrt{3}$, or they could create deeper voids penetrating into the Si. The mechanism was identified as field desorption.[22,23] We have adopted their approach in order to create patterns of artificial defects in the $\sqrt{3}$.

Our experiments were carried out in an ultrahigh vacuum chamber that housed an Omicron variable-temperature STM.

[a)]Present address: Department of Chemical Engineering, Massachusetts Institute of Technology, Cambridge, MA 02139.
[b)]Author to whom correspondence should be addressed; electronic mail: thiel@ameslab.gov

The chamber pressure did not exceed 1.0×10^{-10} mbar throughout the experiments. Most instrumentation and procedures have been described elsewhere.[20,24,25] Specifically in the present work, the $\sqrt{3}$ surface phase was prepared by depositing ~1 ML of Ag on the Si(111)-(7 × 7) and annealing for 2 min at 800 K. This surface was then patterned using a program sequence developed within the Omicron software environment. Individual features (dots) were made by applying a single voltage pulse of +4 V to the tip for 10 ms at room temperature.[22] Lines were drawn using a dense, linear set of 80 individual pulses separated by 1 nm. Larger and deeper features (pits) were made by applying a rastered sequence of 500 × 500 individual pulses within a 10 × 10 nm^2 surface region. The feedback loop was on during all these processes, with current set at 0.2–0.4 nA. Subsequent imaging was done at −2 to + 0.2 V tip bias, and at 2–0.2 nA tunneling current. Ag was deposited on the patterned surface at 300 K, with a typical flux of 0.0067 ML/s. The STM tip was withdrawn during Ag deposition to avoid shadowing effects. After Ag deposition, the original region on the surface was located by using certain features as landmarks at low magnification, and iteratively increasing magnification. The STM tip, used for both imaging and patterning, was electrochemically etched W wire. We found that tip sharpness and stability were very important, in agreement with RCRG.[22] Unstable tips or tips with poor geometry could not make clean, reproducible patterns or were ineffective in subsequent imaging.

Figure 1 shows STM images of dots and a pit, together with line profiles. Dots (single-pulse features) have widths in the range 3–4 nm, and measured depths in the range from −0.1 to −0.3 nm. The average depth is -0.21 ± 0.05 nm. Like RCRG,[22] we do not see evidence that the displaced material accumulates at the edges of the dots. They attributed this to field desorption of (primarily) Si onto the tip, and we also see evidence of this effect. The pits (the rastered-pulse features) have a nominal width of 10 nm and a maximum depth of 1.0–1.2 nm. Further, the floor of the pit is always deeper along a strip that runs down the center, than it is near the sides.

RCRG[22] showed that there is a threshold voltage for field desorption from the $\sqrt{3}$ surface, for a given set of gap conditions. Just above this threshold voltage, the measured width and depth of the defects increased linearly with pulse voltage, and then reached limiting values. They showed that in the regime of linear increase, it was possible to remove a combined Ag–Si layer with a depth of 0.31 nm.[22] In our data, the measured depth of the dots is 0.21 ± 0.05 nm. The pit, however, is deeper (at the center) than the dot by a factor of ~5, and is clearly rough. This may be due to the effect of overlapping field desorption areas in the raster.

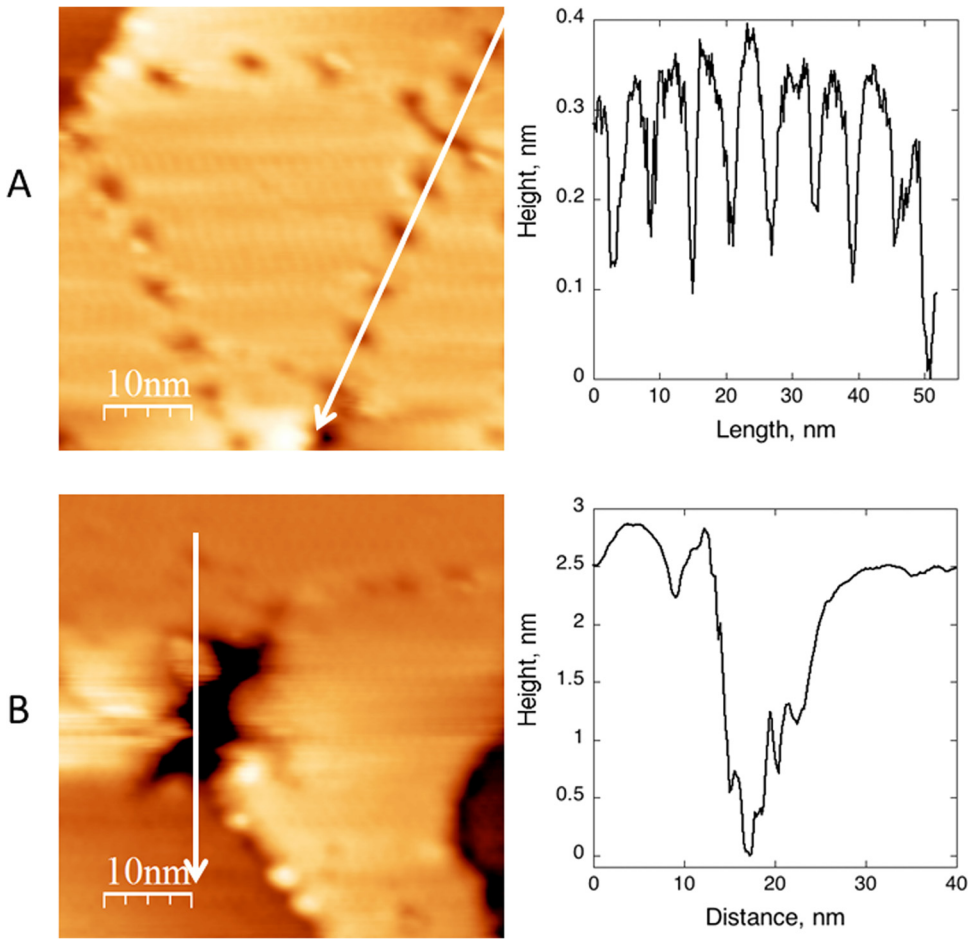

FIG. 1. (Color online) (A) Image and line profile of a set of dots in the $\sqrt{3}$ surface, before Ag deposition. Image size 50 × 50 nm^2. Imaged at 0.2 V, 2 nA. (B) Image and line profile of a pit created in the $\sqrt{3}$ surface, before Ag deposition. Image size 50 × 50 nm^2. Imaged at −0.2 V tip bias, 2 nA tunneling current.

Figure 2 shows STM images of dots and a pit after Ag deposition. Ag collects at these artificial defects, whereas the rest of the surface remains flat and clear; hence confirming the original hypothesis that the deposited Ag is selectively trapped at artificial defects. Figure 2(A) shows the same triangular array of dots as in Fig. 1(A), after 3.25 ML of Ag has been deposited on the surface. Most of the original depressions have turned into protrusions. Figures 2(B)–2(E) show the change in pit morphology with increasing Ag coverage. Ag covers the pit, forming mounds that become larger as Ag coverage increases. Note that Ag in the pit forms different grains, which must grow at different rates, as the grains achieve different heights. In subsequent analysis we will take the height of such a rough cluster of grains as the maximum height.

Figures 3(A) and 3(B) illustrates the changes in height and area of the dots and pits, in response to Ag deposition. Note that the areal dimensions should be taken with caution. The measured shape of small protrusions or voids is actually a convolution of the tip shape and the true shape of the object. Therefore, the true area of the Ag clusters is probably smaller than the measured dimensions by an amount, which in turn depends on the height and pitch of the object. Trends in area are more reliable than absolute values. Unlike area, height is given accurately by the measured value.

According to the data in Fig. 3(A), the dots saturate rather quickly with Ag. They reach an average height of 0.25–0.3 nm within the first 0.5 ML of Ag, and are constant after that. A few dots reach a height of 0.6 nm, but they are not stable under scanning conditions, as a 0.6 nm dot in one image will transform into a 0.3 nm dot in the next image. The area increases gradually with Ag coverage, exceeding the initial area of the empty dot by only 30% at the end of the experiment.

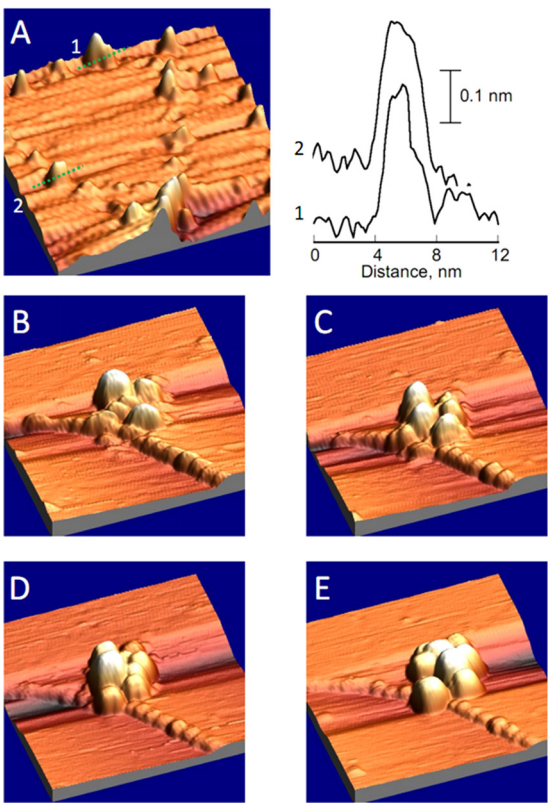

FIG. 2. (Color online) (A) Dots, at 3.25 ML Ag, 50×50 nm^2 image size. Imaged at -1 V, 2 nA. Two typical profiles are shown on the right. (B–E) Pit, at Ag coverages of 0.5, 1, 2, and 3.3 ML. Images are 50×50 nm^2, -1 V, 2 nA.

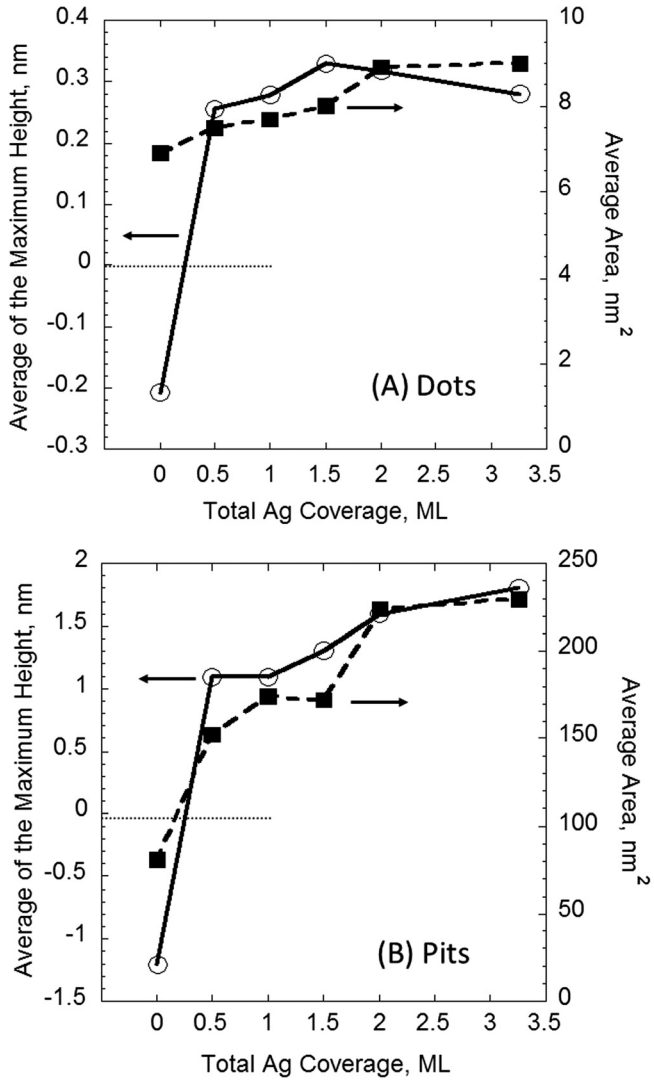

FIG. 3. Maximum heights and measured areas of (A) dots and (B) pits. Heights are represented by circles connected with solid lines, and areas by squares with dashed lines. Both values are measured with respect to the surrounding $\sqrt{3}$. Error bars are not shown to preserve visual clarity. In (A) they are $\sim\pm0.1$ nm in height and ±3 nm^2 in area. In (B) they are $\sim\pm0.5$ nm in height and ±20 nm^2 in area. Negative values of height indicate empty dots or pits, i.e., depressions in the surface, whereas positive values indicate protrusions formed by Ag clusters. In each, the dotted horizontal line emphasizes the zero point for the height axis.

Ag grows at the pit somewhat differently than at the dot. This observation mainly rests on the height of Ag at the pit, which increases more continuously and achieves a much larger value than at the dot. It reaches $\sim$1.8 nm at the highest measured Ag coverage. This suggests that the nucleation and growth of Ag depends sensitively on the characteristics of the artificial defect.

Another difference lies in the measured area of the Ag cluster. Area grows more strongly with total Ag coverage at the pit [Fig. 3(B)] than at the dot [Fig. 3(A)]. At the highest Ag coverage, it exceeds the area of the empty pit by a factor

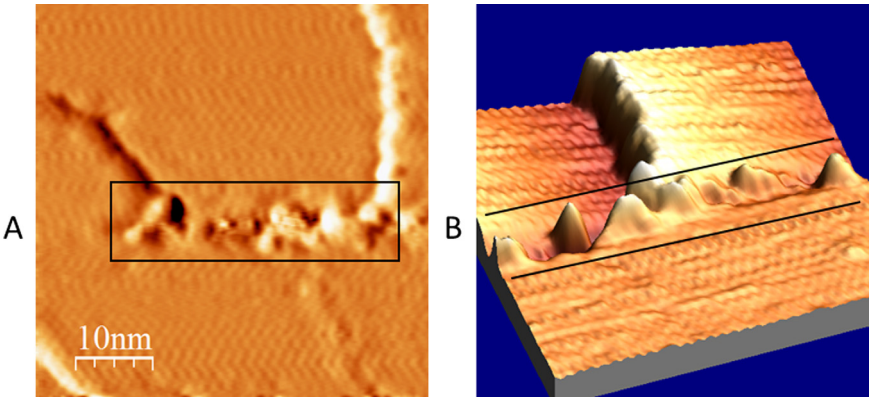

FIG. 4. (Color online) STM images of a single linear array of dots, before and after Ag deposition on the $\sqrt{3}$. Both images are 50×50 nm^2. In both images, some of the intrinsic island–hole boundaries are visible. (A) Linear array of dots patterned on the $\sqrt{3}$, enclosed by black box. Raw STM image at −0.2 V, 2 nA. (B) Same linear array, enclosed by black lines, after deposition of 3.3 ML Ag on the patterned $\sqrt{3}$. Three-dimensional view of the STM image at −1 V, 2 nA.

of 3. This may be due, in part, to the tip artifact mentioned previously. However, continuing growth of the Ag cluster at the pit is easily verified by visual inspection of Figs. 2(B)–2(E). As noted previously, the floor of the dot may be relatively smooth compared with the floor of the pit, and this may account for the different influence on Ag cluster shape.

Finally, the ability to create features in the shape of lines is also technologically important. Figure 4 shows a line of dots before and after adsorption of Ag. The dots are 1 nm apart. Clearly, Ag selectively fills these artificial defects just as it selectively fills the individual dots and the pit. This shows that it is possible to create a sequence of closely spaced Ag clusters that could potentially be transformed into a "wire," with thermal treatment or applied voltage.

There are many other STM-based methods for creating patterns of metal nanoclusters on surfaces.[3] However, the central principle of our technique, i.e., self-assembly at artificial defects, has not been applied previously to metals-on-semiconductors to our knowledge. This is presumably because the diffusion length of metals-on-semiconductors is usually not very large. Ag on the $\sqrt{3}$ surface is exceptional in that regard, with a diffusion length on the order of a micron at 300 K.

For metals-on-semiconductors, one established method of creating arrays of metal clusters is to use the tip as a source of metal, i.e., to transfer clusters of metal from the tip onto the semiconductor surface at different locations.[3,5,6] Another established method is to use the electric field at an STM tip to decompose precursor molecules in chemical vapor deposition, with spatial selectivity.[3,7] The lateral dimensions of features produced by these methods is generally $\geq$5 nm.[3] The lateral size of Ag clusters at the dots produced by our method is in the range 3–4 nm at baseline. In this respect, our approach compares favorably with others. However, other methods are more broadly applicable in the sense that they can be applied to many metal–semiconductor combinations, whereas ours is specific to Ag on the $\sqrt{3}$ surface of Ag.

In summary, we have demonstrated that a $\sqrt{3}$ surface can be patterned with three-dimensional Ag clusters that are as small as 3–4 nm in measured diameter. This nanopatterning method exploits long-range diffusion of Ag on the $\sqrt{3}$, combined with preferential nucleation of Ag at defects. It operates at room temperature, in ultrahigh vacuum, and does not involve chemicals or materials other than Ag and Si.

ACKNOWLEDGMENTS

Work at the Ames Laboratory was supported by the Department of Energy–Basic Energy Sciences under Contract No. DE-AC02-07CH11358.

[1]Y. Xia, J. A. Rogers, K. E. Paul, and G. M. Whitesides, Chem. Rev. **99**, 1823 (1999).
[2]B. D. Gates, Q. Xu, M. Stewart, D. H. Ryan, C. G. Willson, and G. M. Whitesides, Chem. Rev. **105**, 1171 (2005).
[3]A. A. Tseng, A. Notargiacomo, and T. P. Chen, J. Vac. Sci. Technol. B **23**, 877 (2005).
[4]O. Custance, R. Perez, and S. Morita, Nature Nanotechnol. **4**, 803 (2009).
[5]A. Houel, D. Tonneau, N. Bonnail, H. Dallaporta, and V. I. Safarov, J. Vac. Sci. Technol. B **20**, 2337 (1991).
[6]D. Fujita, K. Onishi, and T. Kumakura, Jpn. J. Appl. Phys., Part 1 **42**, 4773 (2003).
[7]R. M. Silver, E. E. Ehrichs, and A. L. de Lozanne, Appl. Phys. Lett. **51**, 247 (1987).
[8]S. Pillai, K. R. Catchpole, T. Trupke, and M. A. Green, J. Appl. Phys. **101**, 093105 (2007).
[9]S. Naczas, P. Akhter, and M. Huang, Appl. Phys. Lett. **98**, 113101 (2011).
[10]V. Poborchii, T. Tada, T. Kanayama, and A. Moroz, Appl. Phys. Lett. **82**, 508 (2003).
[11]A. Shibata, Y. Kimura, and K. Takayanagi, Surf. Sci. **275**, L697 (1992).
[12]A. Shibata and K. Takayanagi, Jpn. J. App. Phys., Part 1 **32**, 1385 (1993).
[13]V. G. Lifshits, A. A. Saranin, and A. V. Zotov, *Surface Phases on Silicon: Preparation, Structures, and Properties* (Wiley, West Sussex, UK, 1994).
[14]A. Shibata, Y. Kimura, and K. Takayanagi, Surf. Sci. **303**, 161 (1994).
[15]A. Shibata, H. Kimura, and K. Takayanagi, J. Vac. Sci. Technol. B **12**, 2026 (1994).
[16]K. J. Wan, X. F. Lin, and J. Nogami, Phys. Rev. B **47**, 13700 (1993).
[17]D. W. McComb, D. J. Moffatt, P. A. Hackett, B. R. Williams, and B. F. Mason, Phys. Rev. B **49**, 17139 (1994).
[18]A. Belianinov, B. Ünal, N. Lu, M. Ji, K.-M. Ho, C.-Z. Wang, M. Tringides, and P. A. Thiel, Phys. Rev. B **82**, 245413 (2010).
[19]A. A. Saranin, A. V. Zotov, V. G. Lifshits, J.-T. Ryu, O. Kubo, H. Tani, T. Harada, M. Katayama, and K. Oura, Surf. Sci. **429**, 127 (1999).
[20]A. Belianinov, B. Ünal, K. M. Ho, C.-Z. Wang, J. W. Evans, M. C. Tringides, and P. A. Thiel, J. Phys: Condens. Matter. **23**, 265002 (2011).
[21]S. Jeong and H. Jeong, Phys. Rev. B **81**, 195429 (2010).
[22]M. Riehl-Chudoba, W. Richter, and V. A. Gasparov, J. Appl. Phys. **83**, 2500 (1998).
[23]T. T. Tsong, Phys. Rev. B **44**, 13703 (1991).
[24]B. Ünal, F. Qin, Y. Han, D. J. Liu, D. Jing, A. R. Layson, C. Jenks, J. W. Evans, and P. A. Thiel, Phys. Rev. B **76**, 195410 (2007).
[25]B. Ünal, A. Belianinov, P. A. Thiel, and M. C. Tringides, Phys. Rev. B **81**, 085411 (2010).